JOURNAL OF PROPULSION AND POWER
Vol. 22, No. 1, January–February 2006

Dual-Mode Operation of Stationary Plasma Thrusters

Alexey Lazurenko,* Vanessa Vial,† and Andre Bouchoule ‡
GREMI Laboratory, 45067 Orleans, France
and
Alexandre Skrylnikov,§ Vyacheslav Kozlov,¶ and Vladimir Kim**
RIAME, 125080, Moscow, Russia

The dual-mode operation of a stationary plasma thruster (SPT) has been investigated using the SPT-140 laboratory-model thruster. The SPT-140 is designed for operation at power levels between 4 and 6 kW. The first mode investigated is the standard one that the SPT-140 was optimized for and consists of mass-flow rates of 12–14 mg/s, discharge voltages between 300 and 400 V, thrust levels of 220–320 mN, and specific impulses ranging from 1900 to 2300 s. The second mode corresponds to high specific impulse (over 3000 s) at reduced thrust (less than 140 mN) operation over the same power range as the first mode. In spite of limitations in magnetic field optimization, anode thrust efficiencies over 55% have been obtained in the second mode. The physical features of high-specific-impulse SPT operation are discussed, including the limitations on the mass flow rates for efficient thruster operation and the possible impact of doubly charged xenon ions on Hall thrusters' characteristics. In addition, a thruster scaling analysis is presented that underlines the tendency for high-power thrusters to operate efficiently over a broader range of mass flow rates and discharge voltages than low-power SPTs.

Nomenclature

B, B_r	=	magnetic field induction, radial component of the magnetic field
b_c, d	=	accelerating channel width and its mean diameter, respectively
E_{i0}^{+}	=	mean energy of the singly charged ions
E_z	=	axial electric field
e	=	electron charge module
F	=	thrust
I_d	=	discharge current
I_e	=	electron current
I_i	=	ion current
I_{sp}	=	specific impulse
k, k_L, k_λ	=	numerical factors
k_e	=	factor of electron velocity
k_θ	=	factor of average axial velocity of the singly charged ions
L_i	=	ionization layer length
M	=	ion and atom mass
m	=	electron mass
$\dot{m}$	=	total mass flow rate (through the anode and cathode)
$\dot{m}_a$	=	anode mass flow rate
$\dot{m}_{a\,\min}$	=	minimum anode mass flow rate
$\dot{m}_c$	=	cathode mass flow rate
$\dot{m}_i^{+}$, $\dot{m}_i^{++}$	=	mass flow rate at the exit of the accelerating channel of the singly and doubly charged ions, respectively
n_e, n_i	=	electron and ion number density
P_d	=	discharge power
P_h	=	heat losses
R_p	=	radius of the trajectory around the thruster of the arm with diagnostics
S	=	cross section of ion flux integration in the plume
$S_c = \pi d b_c$	=	accelerating channel cross-section area
U_d	=	discharge voltage
U_f	=	floating potential in the plume
U_{pl}	=	plasma potential in the plume
V_a, V_i, V_e	=	atom, ion, and electron flux velocity in the channel, respectively
V_i^{+}, V_i^{++}	=	singly and doubly charged ion flux velocity in the plume, respectively
V_{i0}^{+}	=	singly charged ions flux velocity on the axis
$\langle V_{iz}^{+} \rangle$, $\langle V_{iz}^{++} \rangle$	=	average axial velocities of singly and doubly charged ion flux, respectively
γ	=	propellant gas ionization efficiency
ΔU	=	potential drop in the ionization layer
δU	=	voltage losses at ion acceleration
η	=	thruster efficiency
θ	=	angle defining a probe position in the plume relative to the thruster axis
λ_i	=	atom free path before ionization
σ_i	=	ionization cross section
σ_V^2	=	spread in velocities of the singly charged ions (variance)
φ_i	=	ion flux density

Received 13 February 2004; revision received 24 May 2005; accepted for publication 25 May 2005.

*Postdoctoral Candidate; lazurenk@cnrs-orleans.fr.
†Ph.D. Student.
‡Emeritus Professor/Team Leader.
§Head of Laboratory, Stationary Plasma Thruster Department.
¶Head, Stationary Plasma Thruster Department.
**Professor/Chief Scientist, Stationary Plasma Thruster Department.

I. Introduction

ELECTRIC propulsion (EP) is being actively developed for routine implementation on satellites and for deep-space missions. Several types of EP have already been used, such as gridded ion thrusters, Hall thrusters, and pulsed plasma thrusters (PPT). Compared with thermochemical thrusters, the acceleration of ionized propellant allows EP to obtain exhaust velocities of at least an order of magnitude higher. The principal interest in EP stems from the corresponding propellant mass savings associated with these high-specific-impulse devices.

Within the EP technologies, Hall thrusters (HT) inherit a long and successful flight history from the Soviet/Russian space program, which has flown the stationary plasma thruster (SPT) variant since 1972.[1] HT implementation on Western satellites or space missions is now underway.[1–3] The interest for HT in space technology is related to several features of these thrusters: 1) much higher specific impulse (>1400 s) in comparison with chemical thrusters (<300 s) with

thrust efficiency ≥50%, thrust level ∼100 mN, lifetime >5000 h at 1.5-kW electric power; 2) relatively simple and robust design providing a gridless ion flow acceleration; and 3) significant inputs from previous experience.

Industrial developments (SNECMA and Astrium) in Europe,[2] Busek, Aerojet and Pratt and Whitney in the United States,[3] and research programs in many countries underlie the present interest in HT technology. A cooperative research program (GDR 2232) on HT development was launched in France, involving several academic research teams in connection with the French Space Agency (CNES) and industry (SNECMA).[4]

Until recently, HTs were considered for specific impulses less than 2000 s. The development of thrusters with higher specific impulse ($I_{sp} \geq 3000$ s) is clearly of interest for orbit and attitude control of long life and high mass satellites. Moreover, higher power thrusters (e.g., 4–6 kW) that operate efficiently in the two modes defined next would be very useful:

1) Mode 1 is characterized by a standard specific impulse (<2000 s) and a thrust large enough (200–300 mN) for orbit raising of Earth-orbiting satellites.

2) Mode 2 is characterized by a high specific impulse (≥3000 s) at reduced thrust, allowing mass saving for long-term missions.

Relevant data for the dual-mode operation of SPTs are presented in this paper. The basic features of the SPT are briefly reviewed in Sec. II. Prior data obtained for high-voltage operation of the midpower SPT-115 laboratory-model thruster are summarized, and results of an experimental study of the dual-mode operation of the higher power SPT-140 laboratory model are presented. This data set corresponds to a wide range of discharge voltage (300–1000 V), specific impulse (1500–3500 s), and discharge power (0.8–4.5 kW) and is used for the general analysis that is presented in Sec. III.

II. Experimental Investigation of the SPT Operation

A. SPT Operating Principle

SPTs were developed on the basis of the so-called ion accelerator with closed electron drift. Figure 1 is a schematic drawing of the SPT. The discharge voltage U_d is applied between an anode (5) that is located at the bottom of an annular ceramic channel (4) and an external hollow cathode (6). The propellant gas (mass flow rate $\dot{m}_a$) is injected through the anode, and a complementary gas flow $\dot{m}_c$ is required for the cathode operation. A mostly transverse magnetic field is applied across the channel by a magnetic circuit (1) and magnetization coils (2–3), with a maximum radial intensity near the channel exit. The reduced longitudinal mobility of electrons in this channel area leads to a localized potential drop on the order of the discharge voltage. Because of the high electron mobility along magnetic field lines, the equipotentials of the electric field are close to the magnetic field lines. In such an "E cross B" configuration, the electrons drift in the azimuthal direction with an average azimuthal velocity of E_z/B_r. Typical values of E_z and B_r lead to average electron energies higher than 10 eV, which means

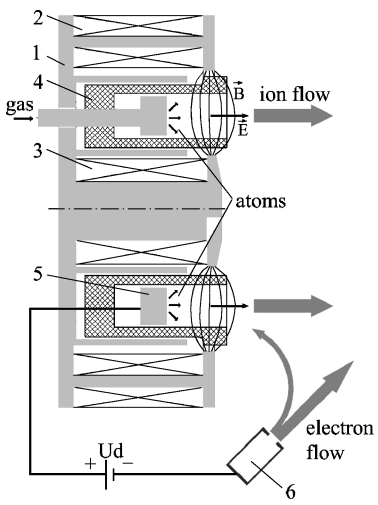

Fig. 1 SPT scheme: 1, magnetic circuit; 2, and 3, magnetization coils; 4, accelerating channel; 5, anode; and 6, cathode.

that this magnetically confined electron cloud is very efficient at ionizing the propellant gas. Xenon (Xe) is generally used as propellant because its high mass leads to a longer residence time in the electron cloud, which together with its low ionization potential improves ionization efficiency. An almost full ionization of the anode Xe flow (typically > 90%) is obtained in optimized SPTs. Xe ions, accelerated towards the exit by the electric field, leave the channel with kinetic energies on the order of the discharge potential. The thrust corresponds to the momentum delivered to this escaping ion flow. The discharge current I_d at the channel exit cross section is the sum of the ion current I_i leaving the channel and the electron current I_e from the cathode entering the channel (primary source of avalanche ionizations). Because the discharge electrical power cost is $U_d I_d = U_d(I_i + I_e)$ while the "useful power" is $U_d I_i$, the lower the electron current, the higher the thrust efficiency. For optimized thrusters the ratio I_e/I_d is typically less than 0.3; most of the cathode electron current is used to neutralize the ion beam flow.

The total mass flow rate through an SPT is $\dot{m} = \dot{m}_a + \dot{m}_c$, where typically $\dot{m}_c \sim 0.1\dot{m}_a$. For a fixed thruster operating mode, the required cathode mass flow rate can vary with cathode design. To characterize the intrinsic thruster performance, we will use in the following the anode mass flow rate as a reference when looking at physical quantities such as the specific impulse and thrust efficiency.

Accordingly, the specific impulse will be defined as

$$I_{sp} = F/\dot{m}_a g \tag{1}$$

and the thruster efficiency as

$$\eta = F^2/2\dot{m}_a P_d = F^2/2\dot{m}_a U_d I_d \tag{2}$$

The power losses in the magnetization coils will not be taken into account in the following discussions because these losses are also design dependent and not intrinsic to the discharge itself.

B. SPT-115 Data over a Wide Voltage Range

Several studies have been devoted to HT operation at high discharge voltage (e.g., Ref. 5–8). The high-voltage performance of the RIAME MAI SPT-80 (Ref. 5), SPT-115 (see the following), and high-power SPT-140 (see Sec. II.C) laboratory model thrusters form a wide ranged database concerning thrusters of different sizes and similar designs that represents a valuable input for insights on performance trends as a function of thruster size and power.

The SPT-80 has a channel external diameter of 80 mm and was designed for the power range 1–1.5 kW. This thruster was operated in an extended range of parameters: anode mass flow rate $\dot{m}_a = 2.1$–9.5 mg/s, discharge voltage $U_d = 100$–800 V, and discharge power $P_d =$ 0.3–3.0 kW.

The SPT-115 has a channel external diameter of 115 mm and internal one of 80 mm. It was designed for the power range of 1.5–3.0 kW and nominal anode mass flow rate range of 8–9 mg/s. The SPT-115 performance at standard conditions ($\dot{m}_a = 8.88$ mg/s, $U_d = 400$ V) is $F = 193$ mN, $I_{sp} = 2190$ s, and $\eta = 62\%$ (Ref. 9).

High-voltage performance characterization of the SPT-115 was made at RIAME MAI in a 2-m-diam by 6-m-long, oil-diffusion pumped test facility. The corrected (for xenon) vacuum chamber background pressure never exceeds $7.5 \cdot 10^{-3}$ Pa for a xenon mass flow rate of 5 mg/s. The corresponding increase of thruster performance related to the neutral backflow at this background pressure is expected to be less than 3% and is neglected.

The discharge voltage and discharge current (precision shunt voltage) are measured by digital voltmeters with a precision better than 0.5%. Internal and external magnetization coils are powered separately by commercially available power supplies that provide both voltage and current indications.

The test facility is equipped with a thrust stand allowing thrust measurement with an accuracy of ±2%. Finally, the gas feed system controls anode and cathode mass flow rates with an accuracy of ±2 and ±4%, respectively. Specific impulse and thruster efficiency are determined within ±4 and ±7%, respectively.

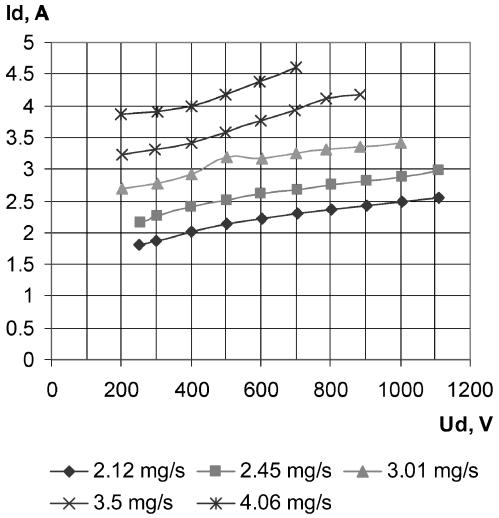

a) SPT-115 voltage-current characteristics

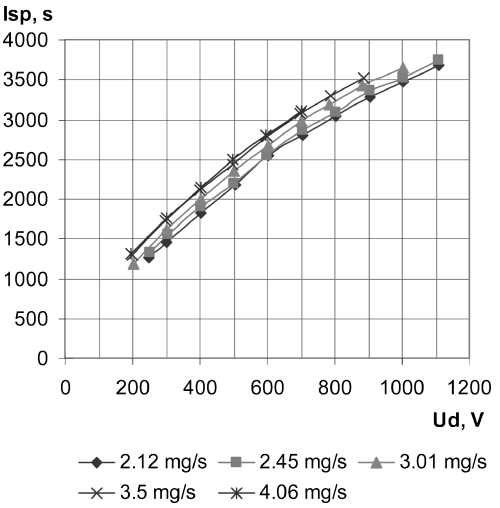

c) SPT-115 anode specific impulse

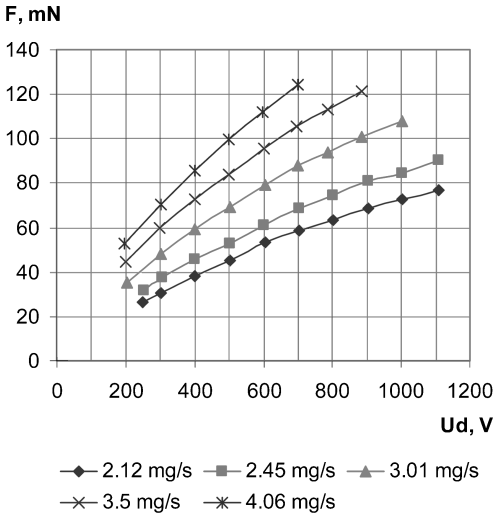

b) SPT-115 thrust

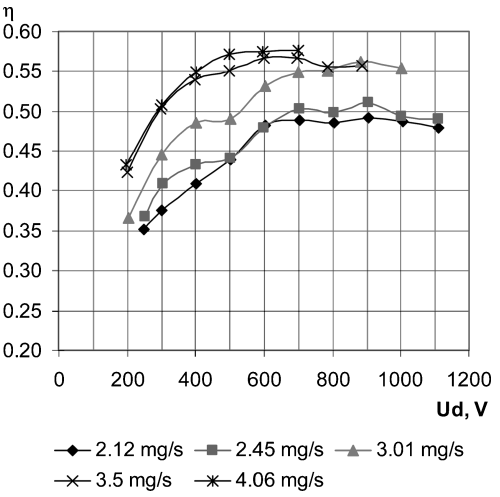

d) SPT-115 anode thrust efficiency

Fig. 2 SPT-115 characteristics for reduced mass flow rates.

SPT-115 data are reported in Figs. 2a–2d for discharge voltages ranging from 200 to 1100 V at reduced anode mass flow rates of 2–4 mg/s.

The discharge current increases with discharge voltage, which appears as typical for SPTs (e.g., Refs. 5–8), although this effect is less pronounced for the SPT-80 (Ref. 5). Several distinct physical sources can be identified for such an increase: increase of the propellant ionization efficiency, increase of the electron current entering the channel, increase of the share of multiply charged Xe ions. These sources will be discussed next. Each operating point was magnetically optimized, that is, recorded with the coil currents adjusted to minimize the discharge current.

Other characteristic features of the SPT-115 can be observed:

1) Thrust and specific impulse increase monotonically with the discharge voltage (see Figs. 2b and 2c) and, in this range of the reduced mass flow rates, I_{sp} increases with $\dot{m}_a$.

2) The maximum value of thrust efficiency shifts into higher discharge voltages when the mass flow decreases (see Fig. 2d).

3) Thrust efficiency is reduced at lower mass flow rates, and a clear trend is observed in terms of voltage—efficiency increases with discharge voltage from the very low initial value 35%, and the discharge voltage at which efficiency saturates decreases with increase of mass flow rate.

Taking into account the preceding data, some general trends in the dual-mode operation of SPTs are apparent:

1) To achieve high thrust at a specified electrical power, it is necessary to operate the thruster with the maximum mass flow rate allowed by the thruster thermal design; that is, at moderate discharge voltages.

2) To achieve high specific impulse under similar thermal limitations, it is necessary to operate the thruster at reduced mass flow rates and high discharge voltages. However, the preceding data show that the reduction of the mass flow rate is limited by a possible decrease of thrust efficiency.

3) A reduction of thrust efficiency induces a limitation on the maximum operating power because of the increased internal losses and possible thermal overloading of the thruster.

Power scale-up trends that are relevant to the just-mentioned observations were examined further with a set of experiments performed on the higher-power SPT-140.

C. Dual-Mode Operation of a High-Power SPT

The RIAME MAI laboratory-model SPT-140 (channel external diameter 140 mm, internal 100 mm) was chosen for these investigations. This model was designed for optimum operation at a discharge power range of 4–6 kW, anode mass flow rates of 12–14 mg/s, and standard discharge voltages between 300 and 400 V (mode 1). In the present study, this thruster was operated in an extended voltage range up to 1000 V, at reduced Xe mass flow rates and at nominal power levels (mode 2).

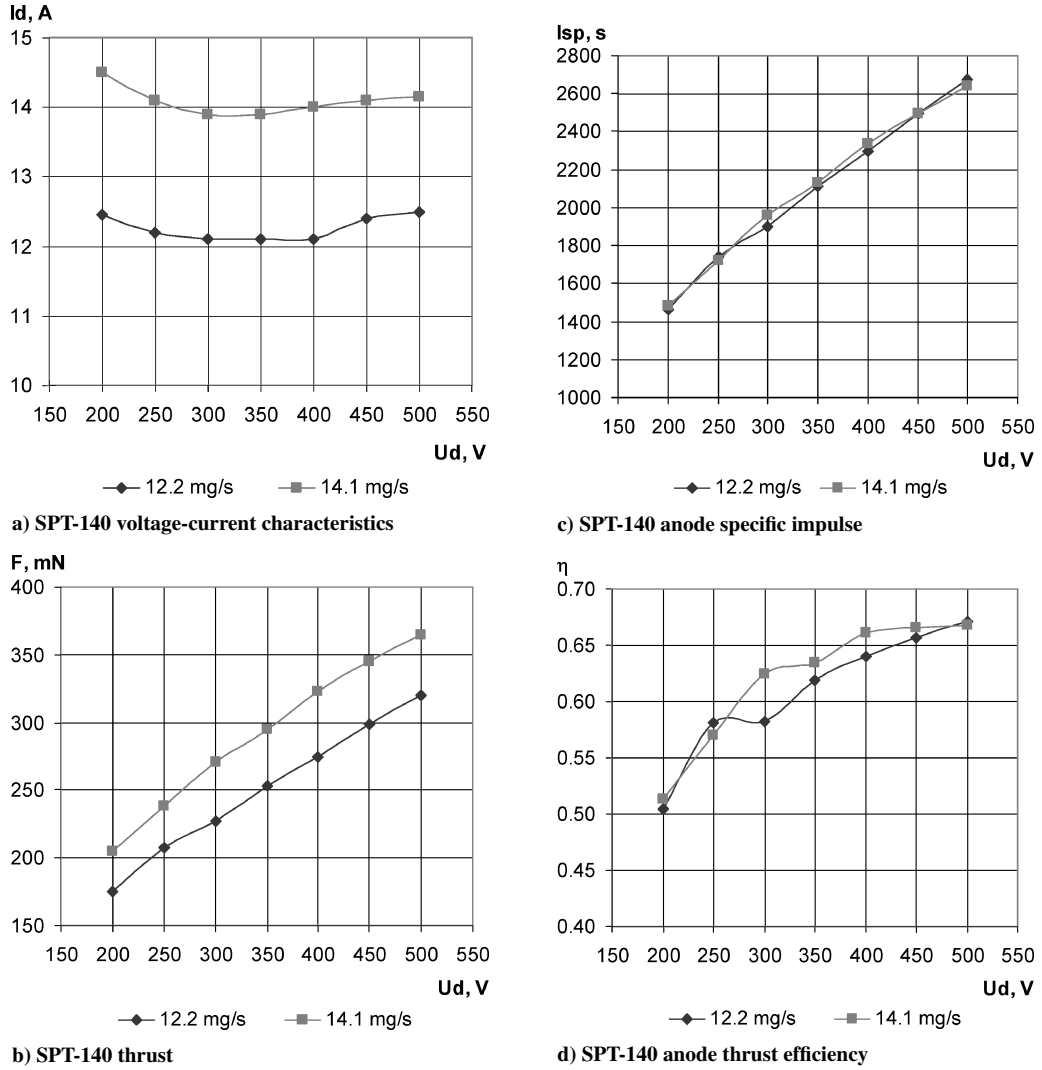

a) SPT-140 voltage-current characteristics

c) SPT-140 anode specific impulse

b) SPT-140 thrust

d) SPT-140 anode thrust efficiency

Fig. 3 SPT-140 mode 1 performance characteristics.

Performance of the SPT-140 operating in mode 1 was recorded at the Kurchatov Institute test facility, where oil-diffusion pumps provide a chamber background pressure of $7.5 \cdot 10^{-3}$ Pa (xenon) for a thruster mass flow rate of 10 mg/s. The results presented in Fig. 3 show that an anode efficiency up to 67% is obtained for discharge power levels up to 7 kW and anode mass flow rates of 12.2 to 14.1 mg/s. At $U_d \approx 300$ V and $P_d \approx 4.2$ kW, the SPT-140 provides a thrust of 270 mN with an anode thrust efficiency of 62% and an anode specific impulse of 1900 s. The SPT-140 efficiency and specific impulse are significantly higher than those of lower-power SPTs. Taking into account the cathode mass flow rate ($\dot{m}_c = 0.1\dot{m}_a$), a specific impulse of 1700 s should be achieved. A similar performance in this power range was also demonstrated in industry: the SPT-140 of Fakel Design Bureau,[10] the PPSX000 of SNECMA,[11] the BPT-4000 of Aerojet.[12]

The performance of the SPT-140 in mode 2 was investigated in the RIAME MAI facility used for the SPT-115 tests (see Sec. II.B).

Data have been acquired for mass flow rates of 3, 3.5, and 4 mg/s over the discharge voltage range of 300 to 1000 V. Internal and external magnetization coils were powered separately by commercially available power supplies. Time-averaged discharge current, thrust, ion current angular distribution in the plume, and plume plasma parameters were recorded. The thruster magnetization currents were adjusted to maximize the thrust efficiency, with limitations at high-voltage and high-power operation. The effect of neutral backflow to the SPT-140 accelerating channel on performance is considered negligible.

The plasma parameters in the plume were recorded by using a cylindrical Langmuir probe (diameter 1.2 mm, length 17 mm). The probe is mounted on a diagnostic rotating arm providing a semicircular trajectory around the thruster at a radius of 0.7 m. The main probe axis is directed along the radius of the semicircle. Plasma potential (with ± 2 V precision) and electron temperature are derived from electrostatic probe data.

The ion current distribution in the SPT-140 plume was recorded by using a retarding potential analyzer (RPA) installed on the same diagnostic arm near the Langmuir probe. The RPA has a stainless-steel housing in which a ceramic body supporting three grids and a collector is installed. The RPA core diameter is 20 mm, and the outer housing is at floating potential. The first grid has 0.225-mm-square holes and is also floating. The second grid, with 0.04-mm-square holes, repels plasma electrons and is set to -37 V relative to the floating housing. The third grid, with 0.266-mm-square holes, is set to $+50$ V relative to the floating potential in order to repel low-energy ions from the ambient plasma. Ion current is received by the collector, which like the grids is made of stainless steel.

The results obtained with the SPT-140 at low mass flow rates are shown in Figs. 4a–4f. Some characteristic data are given here:

1) A thrust efficiency of 56% and a specific impulse of 3640 s are obtained at $U_d = 1000$ V (Figs. 4c and 4d).

2) Unlike the SPT-115, SPT-140 thrust efficiencies at high voltage for mass flow rates of 3.5 and 4 mg/s show no improvement over the efficiencies at 3 mg/s. The observed difference in trends of the two thrusters is thought to be connected with limitations encountered in

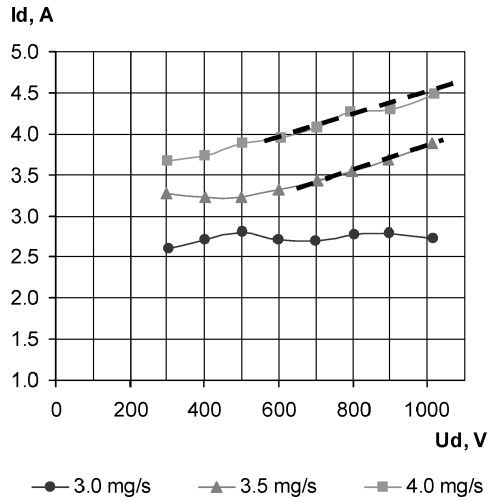

a) SPT-140 discharge characteristics

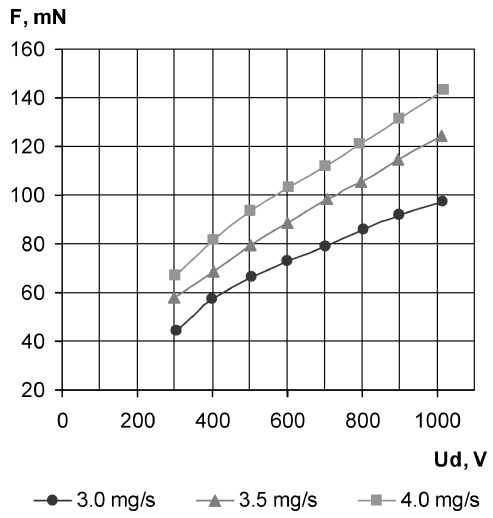

b) SPT-140 thrust

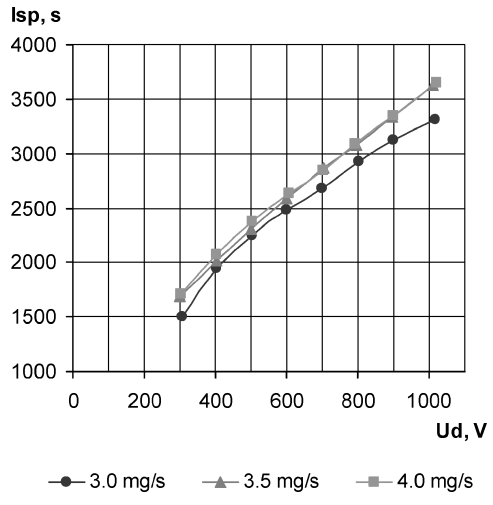

c) SPT-140 anode specific impulse

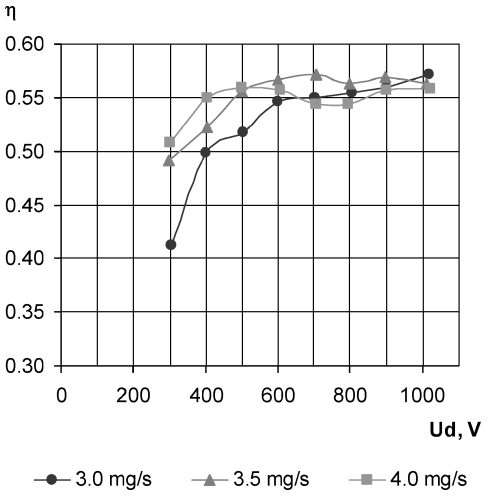

d) SPT-140 anode thrust efficiency

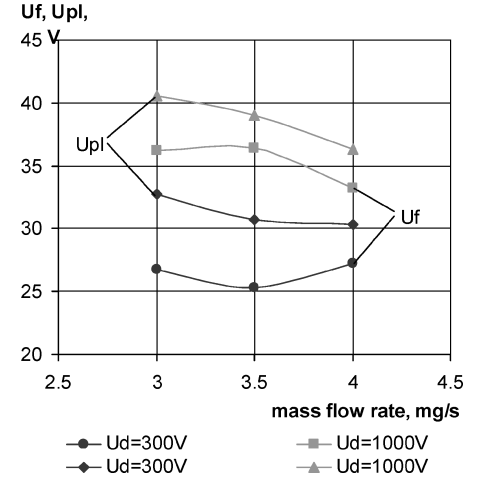

e) SPT-140 floating and plasma potentials on the thruster axis

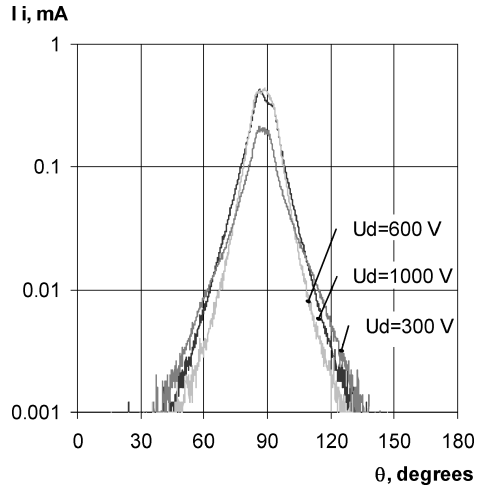

f) Angular distribution of plume ion current; $\dot{m}_a$ = 3.5 mg/s (logarithmic scale)

Fig. 4 SPT-140 mode 2 performance and plume characteristics.

trying to optimize the magnetic field of the SPT-140 at high-voltage, high-power operation modes. Figure 4a shows that the discharge current increases more significantly at high voltage when the mass flow rate (and the thruster power) increases. The optimization of thruster operation at high discharge voltages typically requires an increase of the magnetic field, that is, higher magnetic coil currents.[5–8] However, the magnet power supply used in the present set of SPT-140 experiments is not always able to provide adequate current. The limitation of the coil current is observed at high discharge voltages where the discharge current increases rapidly (indicated by dashed line in Fig. 4a), suggesting nonoptimized thruster operation.

3) The SPT-140 thrust efficiency at discharge voltages between 700 and 1000 V (Fig. 4d) is on the same level as those for smaller SPTs that are optimized for mass flow rates of 3–5 mg/s (e.g., the SPT-80) at discharge voltages of 300–400 V (Ref. 5). The observed increase of thrust and specific impulse with increasing discharge

voltage (Figs. 4b and 4c) suggests that the propellant flow ionization-acceleration processes remain efficient, in spite of the poor magnetic field optimization just reported. The specific impulses obtained for discharge voltages between 700–1000 V are higher for the mass flow rates of 3.5 and 4 mg/s than for 3 mg/s (see Fig. 4c), which follows the same trends observed for the SPT-115.

The main conclusion in terms of mode 2 performance is that even when the magnetic field topology is not fully optimized the SPT-140 can achieve anode specific impulses of 3600 s with anode thrust efficiencies of 55%.

Some physical features related to the thruster plume are described next. The plasma and floating potentials recorded at a distance of 0.7 m from the thruster are shown in Fig. 4e. These data show that plasma potential increases with the discharge voltage, decreases with an increasing mass flow rate, and that the electron temperature remains constant ($\approx$1 eV) in the interrogated operating range. These observations are thought to be connected with electron transport from the cathode to the plume plasma, as suggested by the results of simulation studies,[13] where similar modification of the plasma potential is obtained when the magnetic field increases.

Plume ion current data suggest that most of the ion beam current is concentrated within 45–50 deg of the thruster axis, for the whole voltage range studied.

When recording the SPT-140 performance in a wide operation range, each run duration was limited to the time required for the operation point optimization and discharge parameters stabilization ($\sim$15 min). A test has been done of the thruster operation in mode 2 for longer duration (in two successive runs by 3 h each), where stable thermal conditions were achieved. The operating conditions were a discharge voltage 1000 V, a mass flow rate 3 mg/s, and a discharge power 3 kW. This test demonstrated the ability of the thruster design to operate in mode 2 with stabilized performance such as specific impulse 3250 s and efficiency 50%.

III. Discussion of Dual-Mode SPT Operation

A. Limiting Values of Mass Flow Rate

As just mentioned, operating SPTs at high specific impulse (mode 2) and maintaining mode 1 power level requires a reduced mass flow rate in comparison with a lower specific impulse operation (discharge voltages 300–400 V). Reducing the propellant mass flow rate leads to a decrease of the plasma density in the thruster ionization zone, and the ionization time of Xe atoms can be too high with respect to their residence time in this channel zone. An evaluation of the minimal mass flow required to maintain a high ionization efficiency is given next.

In this analysis we will assume that acceleration occurs mostly downstream of the ionization layer, as evidenced for most SPT designs (for example, see Ref. 14) and suggested by results of numerical simulation.[15,16]

To obtain a high ionization efficiency, the characteristic atom free path for ionization λ_i should be less than the ionization layer length L_i. The former can be expressed as[17]

$$\lambda_i \cong V_a/\langle\sigma_i V_e\rangle n_e \tag{3}$$

At standard discharge voltages $U_d \approx 300$ V, the electron energy can reach 20–30 eV (Ref. 18). Experimental electron-energy distributions are not available for discharge voltages up to 1000 V. Numerical simulations[19–21] predict an almost linear increase of electron temperature with discharge voltage, in the voltage range up to 600 V. This evolution will be assumed next, although it could be a rather rough assumption. Data on xenon ionization cross sections[22,23] show that its variation in the electron-energy range of interest can be neglected when estimating the ionization frequency $\langle\sigma_i V_e\rangle n_e$, in comparison with the corresponding variation of the mean electron velocity $V_e = k_e\sqrt{2eU_d/m}$. The atom velocity V_a will be assumed almost constant in the restricted range of the ceramic channel temperature (500–800 °C).

The plasma density is the most important factor for the evolution of λ_i when the mass flow rate varies. Taking into account plasma quasi-neutrality, the plasma density can be estimated under the assumption of full ionization of propellant gas:

$$n_e \approx n_i \approx \dot{m}_a/MV_iS_c \approx \dot{m}_a/MV_i\pi db_c \tag{4}$$

The averaged ion velocity in the ionization zone V_i is related to the potential drop ΔU in this layer and will be described as

$$V_i = \sqrt{2e\Delta U/M} \tag{5}$$

According to the results of numerical simulation,[15,16] $\Delta U \sim 30$ V for a standard discharge voltage 300 V. These data are in agreement with experimental studies on time-resolved ion-energy distributions, avoiding the broadening effects of thruster fluctuations.[24] The width of the ion-energy distribution in the plume directly reflects the potential drop in the ionization layer. Little information is available on the ion-energy distribution for a wide range of discharge voltages,[25] suggesting that their width does not vary significantly with U_d. This can be expected: the total voltage drop from anode to the thruster plume is mainly achieved in the acceleration domain where the plasma density is significantly lower than in the ionization layer. So, we will assume $V_i =$ const when U_d varies.

In agreement with previous studies,[17] the ionization layer length is assumed to be proportional to the accelerating channel width: $L_i \approx kb_c$. This is related to the fact that increasing the accelerating channel width leads to a corresponding increase of the gap between internal and external poles and the midwidth of the magnetic field intensity distribution along the thruster axis increases as well. The corresponding smoothening of magnetic gradients leads in turn to an extension of the ionization layer length. Other considerations on the influence of the magnetic field topology on the ionization and acceleration processes can be found in Refs. 26 and 27, where the concept of the magnetic field lens or plasma lens is discussed.

The condition of effective ionization will be expressed by $\lambda_i \approx k_L L_i$, where $k_L < 1$. Taking into account the preceding relation of the ionization layer length and the channel width, it can be written as $\lambda_i \approx k_\lambda b_c$. Then, the minimal mass flow rate $\dot{m}_{a\,\min}$ leading to an efficient ionization can be derived from Eqs. (3–5):

$$\dot{m}_{a\,\min} = \left(k_\lambda V_a\sqrt{\Delta U}\Big/\langle\sigma_i\rangle\right)\left(\pi d\Big/\sqrt{U_d}\right)\sqrt{Mm} \tag{6}$$

This expression shows that the minimum mass flow rate ensuring effective propellant flow ionization should decrease when increasing the discharge voltage. Or, under fixed mass flow rate, a decrease of the discharge voltage can induce a decrease of ionization and thrust efficiencies when criterion (6) is not satisfied. These features are qualitatively confirmed by the experimental data given in Sec. II. As can be seen in Fig. 2d, a significant decrease of thruster efficiency is obtained at reduced voltages when the mass flow decreases. The lower the mass flow, the higher the voltage required to restore a better efficiency.

The minimal mass flow rate can be derived quantitatively from Eq. (6) for the SPT-115 thruster where magnetic optimization was not prevented by thermal limitations. The mean diameter is 9.75 cm, and we will assume a ceramic channel temperature of 550°C. The various scaling factors involved in Eq. (6) are estimated here:

1) The ionization cross section in the electron energy range of interest is fixed at $\sigma_i = 4.5 \cdot 10^{-20}$ m^2 (Refs. 22 and 23).

2) The electron velocity is defined by assuming a reasonable energy of 20 eV for a discharge voltage of 350 V [i.e., $V_e = 1.55 \cdot 10^5 (U_d)^{1/2}$].

3) The value of ΔU is fixed at $\Delta U = 30$ V (as just discussed).

4) The product of the geometrical factors k and k_L is assigned to be $k \cdot k_L = 0.8 \cdot 0.5 = 0.4$ (i.e., an effective ionization length $\lambda_i = 7$ mm).

These values lead to a quantitative expression of the minimum mass flow rate given by $\dot{m}_{a\,\min} = 50(U_d)^{1/2}$, where the mass flow is expressed in milligrams/second and the discharge voltage in volts. For $U_d = 500$ V this estimation leads to a minimal mass flow rate of 2.3 mg/s. One can see in Fig. 2d that the significant decrease of efficiency observed for this thruster at the mass flow rate between 2 and 4 mg/s is in rather good agreement with the preceding criterion. The

range of thruster voltages where a significant drop of efficiency is observed cannot be described by such a model assuming an almost full ionization efficiency, but its displacement towards higher energies when the mass flow rate decreases is qualitatively in agreement with the model.

The mass flow rate for mode 1 operation is mostly related to thermal issues. The part P_h of the discharge power P_d transferred into heat (radiation, wall recombination and ionic impacts) depends on the optimization of thruster design and operation mode and could be assumed to be proportional to P_d: $P_h \propto P_d = I_d U_d$. If we further assume $I_d \propto \dot{m}_a$, then $\dot{m}_a \propto P_h/U_d$. For a specified thermal power, supported by the thruster, the mass flow rate varies as $1/U_d$.

It is also interesting to look at the effect of up-scaling on the maximal discharge voltage acceptable from the thermal considerations. Let us introduce the mass flow density calculated for the thruster cross-section area $S_c = \pi d b_c$. Assuming the discharge current to be proportional to the mass flow rate, one can obtain from Eq. (6):

$$I_d/S_c \propto \dot{m}_{a\,\min}/S_c = \left(k_\lambda V_a \sqrt{\Delta U}\Big/\langle\sigma_i\rangle\right)\left(\sqrt{Mm}\Big/b_c\sqrt{U_d}\right) \quad (7)$$

where the minimal mass flow density is inversely proportional to b_c. Equation (7) shows that the acceptable minimum of the discharge current density is reduced with increase of the accelerating channel width. Or, for a fixed power density (limited by thermal issues), such a decrease of discharge current density allows an increase of the discharge voltage maintaining high values of ionization and thrust efficiency.

The up-scaling trends just derived are consistent with experimental data. Table 1 gives an overview of data for the three thrusters SPT-80, SPT-115, and SPT-140 investigated in a wide range of voltage and mass flow rate.

The minimum mass flow rate required for efficient ionization increases linearly with the channel width b_c [see Eq. (6)]. The mass flow rates at standard mode 1 operating points for the SPT-80, SPT-115, and SPT-140 thrusters lead to the $\dot{m}_a/S_c$ values, which increase faster then the channel cross section (see Table 1). These considerations show that the relative range of mass flow rates $\dot{m}_a/\dot{m}_{a\,\min}$, where the thruster can be operated efficiently, increases with thruster size and thruster power. This fact is also highlighted by the efficiency trends for the just-mentioned thrusters given in Figs. 5 and 6. The thrust efficiency is represented as a function of the mass flow rate normalized to the standard one for each thruster (see Table 1).

These data confirm that higher power thrusters can be operated over a wider relative range of mass flow rates, and they are of interest for a dual-mode operation with high specific impulse and good thrust efficiencies.

B. Analysis of the Discharge Current and Thrust Trends

The set of experimental data presented in Sec. II was analyzed in an attempt to explain some observed features. Discharge current shows more or less pronounced increase with discharge voltage (see Fig. 2a for the SPT-115, Fig. 4a for the SPT-140). This behavior appears to be a general property of Hall thrusters (see Refs. 5–8), even at the magnetically optimized operation points. Such an increase leads to higher discharge power and effects negatively the thruster efficiency if it is not related to a simultaneous increase of ion current and thrust [see Eq. (2)].

The discharge current is $I_d = I_i + I_e$. An increase of the electron contribution I_e can be induced by a less efficient magnetic optimization. An increase of the ion contribution I_i can be induced by two phenomena. The first one is an increase of the ionization efficiency of the gas flow when the voltage increases: as was shown in the preceding paragraph, the critical mass flow rate ensuring effective ionization decreases with increasing discharge voltage. The second phenomenon is a possible increase of the contribution of doubly charged ions in the total ion current. Indeed, recent data show that multiply charged ion fraction increases with discharge voltage.[28]

Table 1 Comparative data on dual-mode operation of SPT laboratory models

Operating parameter/ characteristic	SPT-80		SPT-115		SPT-140	
	Mode 1	Mode 2	Mode 1	Mode 2	Mode 1	Mode 2
$\dot{m}_a$, mg/s	3.15	2.1	8.88	3.01	14.1	3.5
$\dot{m}_a/S_c$ mg/(s · cm^2)	0.123	——	0.168	——	0.185	——
U_d, V	300	600	300	800	300	1000
I_{sp}, s	1630	2400	1830	3200	1950	3640
η, %	48	52	57	55	62	56

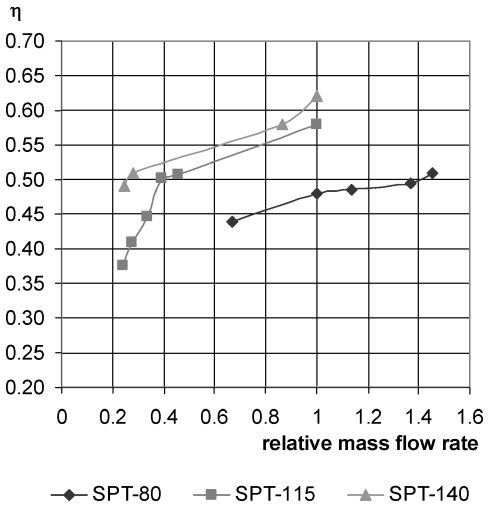

Fig. 5 Thrust efficiency vs relative mass flow rate at $U_d = 300$ V.

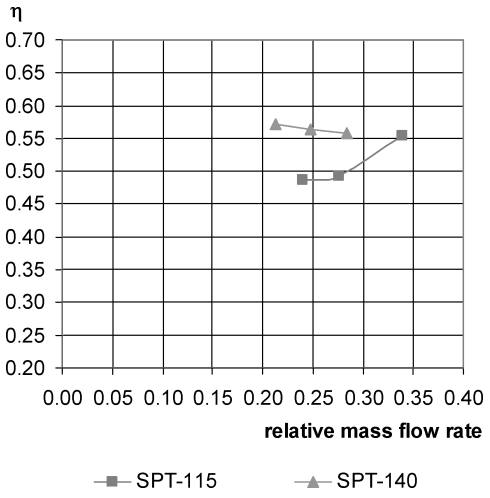

Fig. 6 Thrust efficiency vs relative mass flow rate at $U_d = 1000$ V.

The experimental data for the SPT-140 and the SPT-115 were used for an examination of these various contributions in the thruster current.

To simplify, let us consider only the presence of singly (Xe^+) and doubly charged (Xe^{++}) ions.

The thrust is expressed as

$$F = \dot{m}_i^+ \left\langle V_{iz}^+ \right\rangle + \dot{m}_i^{++} \left\langle V_{iz}^{++} \right\rangle \quad (8)$$

The discharge current is

$$I_d = I_i + I_e = \left(\dot{m}_i^+ + 2\dot{m}_i^{++}\right)(e/M) + I_e \quad (9)$$

The mass flow rates $\dot{m}_i^+$ and $\dot{m}_i^{++}$ of Xe^+ and Xe^{++} ions leaving the thruster are defined as

$$\dot{m}_i^+ + \dot{m}_i^{++} = \gamma \dot{m}_a \quad (10)$$

The average axial velocity of the singly charged ions is defined as

$$\left\langle V_{iz}^+ \right\rangle = \frac{\int_S \left(\varphi_i V_i^+\right)_z \, \mathrm{d}S}{\int_S \varphi_i \, \mathrm{d}S} \quad (11)$$

involving the integral of the ion flux density φ_i through a cross section S of the thruster plume. The surface S in Eq. (11) is a semispherical one centered on thruster output and with the radius R_p. Assuming azimuthal symmetry of the plume, the average axial velocity can be written as

$$\left\langle V_{iz}^{+}\right\rangle = \frac{\int_0^{\pi/2} \varphi_i V_i^{+} \cos\theta \sin\theta \, \mathrm{d}\theta}{\int_0^{\pi/2} \varphi_i \sin\theta \, \mathrm{d}\theta} \tag{12}$$

In this expression V_i^+ is the projection of the local Xe^+ flux velocity along the radial direction defined by θ. In spite of the finite value of the measurement radius R_p, V_i^+ is assumed to be in the radial direction. A significant deviation of ion flux from the radial direction can arise at wide angles ($\theta > 45$ deg) (Ref. 29). In most thrusters more than 90% of the ion flux is launched within a cone of 45–50 deg and the preceding approximation is rather good.

We will take into account the angular variations of the ion beam energy, reported in many papers.[30,31] The energy decreases from maximal values for $\theta = 0$ deg down to one-half of this value for $\theta = 45$ deg. Accordingly we will assume that V_i^+ is described by an angular variation such as $V_i^+ = V_{i0}^+ \cos\theta$, where V_{i0}^+ is the ion flux velocity on the axis (at $\theta = 0$ deg). This angular dependence leads to the expected decrease of the kinetic energy by a factor 2 at 45 deg and to a cancellation of the ion flow at 90 deg.

Inserted in the definition of the averaged axial velocity Eq. (12), this angular dependence leads in a straightforward way to the following relation:

$$\left\langle V_{iz}^{+}\right\rangle = \frac{\int_0^{\pi/2} \varphi_i \cos^2\theta \sin\theta \, \mathrm{d}\theta}{\int_0^{\pi/2} \varphi_i \sin\theta \, \mathrm{d}\theta} V_{i0}^{+} = k_\theta V_{i0}^{+}$$

Data on φ_i have been acquired in the wide operation range of the SPT-140 thruster just reported. The corresponding values of k_θ vary from 0.882 to 0.954.

The evaluation of the mean ion velocity on the axis is derived from RPA data. The energy distribution is defined by a mean value E_{i0}^+ and an energy spread. The theory of random variables leads to the relation

$$\left(V_{i0}^{+}\right)^2 = \left\langle V_{i0}^{+2}\right\rangle - \sigma_V^2$$

In agreement with available data,[25,30,32] we will use in the following an ion mean energy on the axis $M\langle V_{i0}^{+2}\rangle/2$ defined as $E_{i0}^+ = e(U_d - \delta U)$ with a constant value of a few tens of volts for δU. The term σ_V^2 is defined by the Xe^+ ion kinetic energy distribution. The impact of the discharge voltage on the half-width at half-maximum (HWHM) of this distribution was suggested as negligible in Ref. 25 and significant in Ref. 32. When energy distribution is recorded by the RPA technique, Xe^+ and Xe^{++} ions cannot be separated, and an increase of Xe^{++} ions contribution with discharge voltage can lead to an apparent broadening of the Xe^+ energy distribution function. Two approximations have been checked in our following derivations: a constant value of σ_V^2 and a value increasing linearly with discharge voltage, in agreement with Ref. 32. The obtained results on I_e and $\dot{m}_i^{++}$ show the same trends with maximum quantitative discrepancies of less then 10% for I_e and less then 30% for $\dot{m}_i^{++}$. So, the simpler approximation has been used of constant value of $\sigma_V^2 = (2e/M)(\delta U/2)$.

The average axial Xe^+ velocity is derived from the preceding relations:

$$\left\langle V_{iz}^{+}\right\rangle = k_\theta \sqrt{2e/M}\sqrt{U_d - 3\delta U/2} \tag{13}$$

where $U_d - 3\delta U/2$ appears as an "effective" acceleration potential.

The average axial Xe^{++} velocity can be defined through the same approach. Experimental data on both angular and energy distributions at different discharge voltages are not really available for these ions. Such a complete analysis for $U_d = 300$ V was obtained by using an ultrafast anode current interruption. A simultaneous determination of angular and energy distributions was obtained by using time of flight delays for individual data on singly and doubly charged Xe ions.[33] The main result is that the kinetic energy of Xe^{++} ions is slightly less than double the kinetic energy of Xe^+ ions, their energy spread is almost the same, and their contribution to the total ion flow increases with θ at low θ values. These deviations between Xe^+ and Xe^{++} features will be neglected in comparison with the most important effect of kinetic energies, and the average axial Xe^{++} velocity is expressed as

$$\left\langle V_{iz}^{++}\right\rangle = k_\theta \sqrt{2}\sqrt{2e/M}\sqrt{U_d - 3\delta U/2} \tag{14}$$

The total thrust with the use of Eqs. (8), (13), and (14) is expressed as

$$F = \left(\dot{m}_i^{+} + \sqrt{2}\dot{m}_i^{++}\right) \cdot k_\theta \sqrt{2e/M} \cdot \sqrt{U_d - 3\delta U/2} \tag{15}$$

The unknowns in the problem, defined by Eqs. (9), (10), and (15), are $\dot{m}_i^+$, $\dot{m}_i^{++}$, I_e, and the propellant gas ionization efficiency γ.

If γ was known $\dot{m}_i^+$, $\dot{m}_i^{++}$, and I_e could be derived from Eqs. (9), (10), and (15).

In the following analysis we will consider γ as a free parameter within a constrained variation domain. These constraints are the following ones:

1) The γ value must lead to positive values for the three unknowns.

2) The γ is an increasing function of thruster voltage, as the electron energy increases with voltage; we will assume the simplest linear increase from minimal to maximal value when the voltage increases at constant mass flow.

3) Simulation data published for the thruster SPT-100ML operated at 300 V and 5 mg/s (Ref. 16) show that gas ionization efficiency should be as high as 0.96; in the following we will assume that the range of realistic values of γ is 0.78–0.96 in the full range of operation of both the SPT-115 and the SPT-140.

Taking into consideration these constraints on ionization efficiency estimations, the unknowns were derived, and results are shown in Figs. 7 and 8, where the variations of γ, $\dot{m}_i^{++}$, and I_e are presented. In these calculations $\delta U = 30$ V.

In Eq. (15) describing the thrust, it is clear that the most important source of uncertainty is the factor k_θ involving both angular and energy distributions. As precise experimental data are not available, we checked the sensitivity of the results to the value of this parameter: solid lines for $k_\theta = 0.92$ and dashed lines for $k_\theta = 0.95$ in Fig. 7. It is clear that precise experimental insights on Xe^+ and Xe^{++} ions in the thruster plume are required for the sake of precision in these derivations. Similarly, a precise value of I_e is not really available (lack of absolute precision in the determination of the total ion current leaving the thruster channel).

Nevertheless some clear trends are evidenced through the results of this analysis:

1) It is clear that the Xe^{++} contribution is to be taken into account in any case for the interpretation of thruster data such as current and thrust.

2) The I_e contribution of the SPT-140 increases as expected in the domain, where a good optimization is prevented by magnetic limitations.

3) When looking at SPT-140 and SPT-115 results for the same mass flow rate of 3 mg/s, a higher contribution of Xe^{++} is observed for the latter; its channel cross section being smaller by a factor $\sim$1.5, the higher plasma density clearly enhances the probability of a second ionization.

4) The Xe^{++} contribution appears to be rather high but several results in the literature also suggest a significant contribution,[25,28] and this contribution appears to increase with the discharge voltage as evidenced also experimentally.

The main conclusion of the present analysis is that, in spite of an evident lack of precise data on both angular and energy ion distributions in plume, the interpretation of current and thrust data for SPTs requires accounting for multiply charged Xe ions.

A second conclusion is that higher size (and power) thrusters can be operated in the low mass flow rate range with a lower contribution of these energetic species.

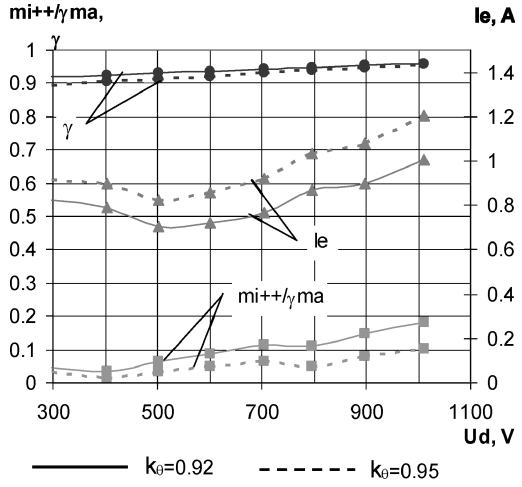

a) $\dot{m}_a = 3.5$ mg/s

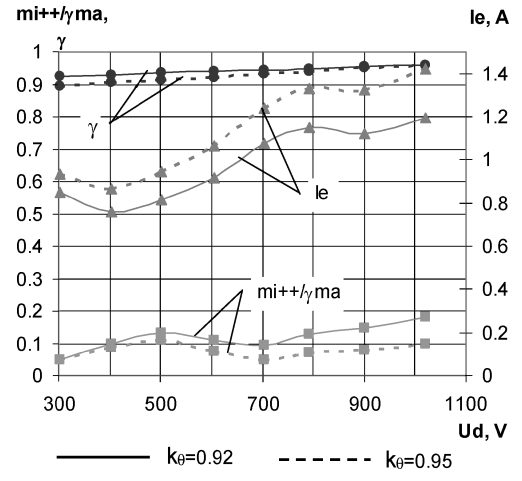

b) $\dot{m}_a = 4$ mg/s

Fig. 7 Doubly charged ion fraction, propellant gas ionization efficiency, and electron current for the SPT-140.

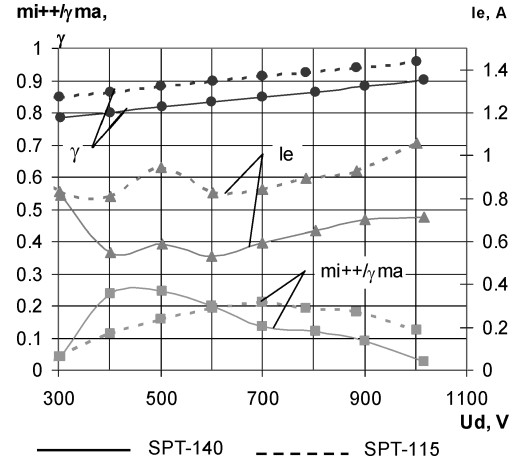

Fig. 8 Doubly charged ion fraction, propellant gas ionization efficiency, and electron current for the SPT-140 and the SPT-115 at $\dot{m}_a = 3$ mg/s, $k_\theta = 0.95$.

IV. Conclusions

Together with the new experimental data reported here, a wide range of data was available for three thrusters of similar design with various sizes and powers. These data have been examined in terms of dual-mode operation. The high-power SPT-140 laboratory model, designed and optimized for low-specific-impulse, high-thrust operation ($P_d = 4$–6 kW, $I_{sp} = 1900$–2300 s, $F = 220$–320 mN), has shown specific impulse over 3000 s and anode thrust efficiency 55% when operated at this power level but under discharge voltages up to 1000 V. Limitations of the high-specific-impulse operation (mode 2) of this thruster were experimentally evidenced. This means that thrusters designed for dual-mode operation should have a specific magnetic (and thermal) design to prevent such limitations. In terms of scaling trends, an increase in thruster size (and power) is beneficial for a dual-mode operation and is also welcome in terms of efficiency. An analysis of such up-scaling trends appears to be in reasonable agreement with experimental data. In any Hall thruster the composition of the ion jet appears an important issue. An examination of experimental data shows that the impact of Xe^{++} ions on thruster features cannot be neglected, even if a clear lack of data prevents a more precise evaluation of this impact. An interesting trend is the possible reduction of such an impact when thruster size increases. The main conclusion is that high power Hall thrusters are interesting candidates for high specific impulse and/or dual-mode electric propulsion.

Acknowledgments

The study on high-power, high-specific-impulse stationary plasma thruster (SPT) was achieved with the support of the ESTEC ESA ("DMHPSPT" GREMI Contract No. 16218/NL/PA). The participation of A. Lazurenko was funded by a fellowship from the Centre National d' Etudes Spatiales (CNES), France. The participation of V. Vial was funded by a fellowship from the SNECMA and the CNES, France. The authors would like to thank the Research Institute of Applied Mechanics and Electrodynamics of Moscow Aviation Institute staff, namely, Dmitry Grdlichko and Lev Umnitsyn for this opportunity to investigate the dual-mode SPT concept. The authors wish to thank the reviewers for their detailed and welcome comments. The help of the Associate Editor and other experts in improving the English language up to the standard required by the journal is also appreciated.

References

[1]Kim, V., Popov, G., Tikhonov, V., Garkusha, V., and Murashko, V., "Modern Trends of Electric Propulsion Activity in Russia," *International Electric Propulsion Conference*, Paper 99-004, Oct. 1999.

[2]Saccoccia, G., "Introduction to the European Activities in Electric Propulsion," *International Electric Propulsion Conference*, Paper 03-341, March 2003.

[3]Myers, R. M., "Overview of Major U.S. Industrial Programs in Electric Propulsion," AIAA Paper 2000-3147, July 2000.

[4]Cadiou, A., Darnon, F., and Jolivet, L., "An Overview of the CNES Electric Propulsion Program," *International Electric Propulsion Conference*, Paper 03-169, March 2003.

[5]Kim, V., Kozlov, V., Lazurenko, A., Popov, G., Skrylnikov, A., Clauss, C., Day, M., and Sancovic, J., "Development and Characterization of Small SPT," AIAA Paper 98-3335, July 1998.

[6]Manzella, D. H., Jacobson, D. T., and Jankovsky, R. S., "High Voltage SPT Performance," AIAA Paper 2001-3774, July 2001.

[7]Pote, B., and Tedrake, R., "Performance of a High Specific Impulse Hall Thruster," *International Electric Propulsion Conference*, Paper 01-35, Oct. 2001.

[8]Hofer, R. R., and Jankovsky, R. S., "The Influence of Current Density and Magnetic Field Topography in Optimizing the Performance, Divergence, and Plasma Oscillations of High Specific Impulse Hall Thrusters," *International Electric Propulsion Conference*, Paper 2003-142, March 2003.

[9]Kim, V., Grdlichko, D., Kozlov, V., Lazurenko, A., Popov, G., Skrylnikov, A., and Day, M., "SPT-115 Development and Characterization," AIAA Paper 99-2568, June 1999.

[10]Gnizdor, R., Kozubsky, K., Maslennikov, N., Murashko, V., Pridannikov, S., and Kim, V., "Performance and Qualification Status of Multimode Stationary Plasma Thruster SPT-140," *International Electric Propulsion Conference*, Paper 99-090, Oct. 1999.

[11]Duchemin, O., Dumazert, P., Clark, S. D., and Mundy, D. H., "Development and Testing of a High-Power Hall Thruster," *International Electric Propulsion Conference*, Paper 03-0032, March 2003.

[12]Fisher, J., Wilson, A., King, D., Meyer, S., de Grys, K., and Werthman, L., "The Development and Qualification of a 4.5 kW Hall Thruster Propulsion System for SEO Satellite Applications—Status Update," *International Electric Propulsion Conference*, Paper 03-0295, March 2003.

[13]Keidar, M., and Boyd, I. D., "Effect of a Magnetic Field on the Plasma Plume from Hall Thrusters," *Journal of Applied Physics*, Vol. 86, No. 9, 1999, p. 4786.

[14]Dorval, N., Bonnet, J., Marque, J. P., Rosencher, E., Chable, S., Rogier, F., and Lasgorceix, P., "Determination of the Ionization and Acceleration Zones in a Stationary Plasma Thruster by Optical Spectroscopy Study: Experiments and Model," *Journal of Applied Physics*, Vol. 91, No. 8, 2002, p. 4811.

[15]Kim, V., Bishaev, A. M., Lazourenko, A. V., and Auweter-Kurtz, M., "3-Dimensional Simulation of Plasma Dynamics in SPT," *International Electric Propulsion Conference*, Paper 01-340, Oct. 2001.

[16]Hagelaar, G. J. M., Bareilles, J., Garrigues, L., and Bœuf, J.-P., "Role of Anomalous Electron Transport in a Stationary Plasma Thruster Simulation," *Journal of Applied Physics*, Vol. 93, No. 1, 2003, p. 67.

[17]Kim, V., "Main Physical Features and Processes Determining the Performance of Stationary Plasma Thrusters," *Journal of Propulsion and Power*, Vol. 14, No. 5, 1998, pp. 736–743.

[18]Bishaev, A. M., and Kim, V., "Local Plasma Properties in Hall-Current Accelerator with an Extended Acceleration Zone," *Soviet Physics—Technical Physics*, Vol. 23, No. 9, 1978, p. 1055.

[19]Szabo, J. J., Rostler, P. S., McElhinney, S. A., and Warner, N. Z., "One and Two Dimensional Modeling of the BHT-1000," *International Electric Propulsion Conference*, Paper 03-0231, March 2003.

[20]Ahedo, E., Gallardo, J. M., Parra, F. I., and Pérez Trigo, C., "Recent Results from a Model of the Hall Thruster Discharge," *International Electric Propulsion Conference*, Paper 03-0331, March 2003.

[21]Barral, S., Makowski, K., Peradzynski, Z., Gascon, N., and Dudeck, M., "Wall Material Effects in Stationary Plasma Thrusters. II. Near-Wall and In-Wall Conductivity," *Physics of Plasmas*, Vol. 10, No. 10, 2003, p. 4123.

[22]Syage, J. A., "Electron-Impact Cross Sections for Multiple Ionization of Kr and Xe," *Physical Review A*, Vol. 46, No. 9, 1992, p. 5666.

[23]Rejoub, R., Lindsay, B. G., and Stebbings, R. F., "Determination of the Absolute Partial and Total Cross Sections for Electron-impact Ionization of the Rare Gases," *Physical Review A*, Vol. 65, 2002, p. 042713.

[24]Bouchoule, A., Cadiou, A., Heron, A., Dudeck, M., and Lyszyk, M., "An Overview of the French Research Program on Plasma Thrusters for Space Applications," *Contributions to Plasma Physics*, Vol. 41, No. 6, 2001, pp. 573–588.

[25]Vesselovzorov, E. E., and Svirsky, E. B., "Mass-Charges-Energetically Analysis of Particle Flux of CDEA," *VI All-Union Conference on Plasma Accelerators and Ion Injectors*, Dnepropetrovsk State Univ., USSR, 1986, p. 42.

[26]Gavryushin, V. M., Kim, V., Kozlov, V. I., and Maslennikov, N. A., "Physical and Technical Bases of the Modern SPT Development," *International Electric Propulsion Conference*, Paper 95-38, Sept. 1995.

[27]Hofer, R. R., Peterson, P. Y., Gallimore, A. D., and Jankovsky, R. S., "A High Specific Impulse Two-Stage Hall Thruster with Plasma Lens Focusing," *International Electric Propulsion Conference*, Paper 01-036, Oct. 2001.

[28]Hofer, R. R., and Gallimore, A. D., "Ion Species Fractions in the Far-Field Plume of a High-Specific Impulse Hall Thruster," AIAA Paper 2003-5001, July 2003.

[29]Bishaev, A. M., Kalashnikov, V. K., Kim, V., and Shavykina, A. V., "Numerical Simulation of the Stationary Plasma Thruster Plasma Jet Propagating in the Low-pressure Medium," *Plasma Physics Report*, Vol. 24, No. 11, 1998, pp. 989–995 (in Russian).

[30]King, K. B., and Gallimore, A. D., "Mass Spectral Measurements in the Plume of an SPT-100 Hall Thruster," *Journal of Propulsion and Power*, Vol. 16, No. 6, 2000, pp. 1086–1092.

[31]Askhabov, S. N., Burgasov, M. P., Veselovzorov, A. N., et al., "Study of the Plume of the Stationary Plasma Accelerator with Closed Electron Drift (CDEA)," *Plasma Physics Report*, Vol. 7, No. 1, 1981, pp. 225–230 (in Russian).

[32]Hofer, R. R., Haas, J. M., and Gallimore, A. D., "Ion Voltage Diagnostics in the far-Field of a High-Specific Impulse Hall Thruster," AIAA Paper 2003-4556, July 2003.

[33]Prioul, M., "Experimental Study of Hall Thrusters," Ph.D. Dissertation, Univ. of Orléans, France, Sept. 2002.